

# Polyelectrolyte Adsorption onto Oppositely Charged Interfaces: Image-Charge Repulsion and Surface Curvature

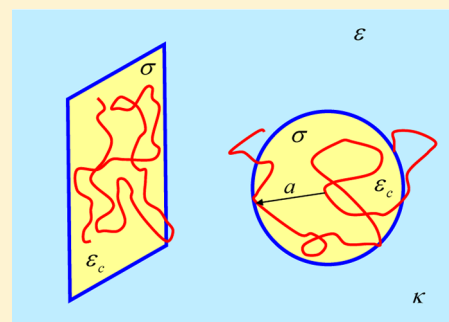
A. G. Cherstvy<sup>\*,†,‡</sup> and R. G. Winkler<sup>§</sup>

<sup>†</sup>Institute for Physics and Astronomy, University of Potsdam, 14476 Potsdam-Golm, Germany

<sup>‡</sup>MPI for Physics of Complex Systems, Nöthnitzerstr. 38, 01187 Dresden, Germany

<sup>§</sup>Theoretical Soft Matter and Biophysics, Institute of Advanced Simulation, Research Center Jülich, 52425 Jülich, Germany

**ABSTRACT:** We analyze theoretically the influence of low-dielectric boundaries on the adsorption of flexible polyelectrolytes onto planar and spherical oppositely charged surfaces in electrolyte solutions. We rationalize to what extent polymer chains are depleted from adsorbing interfaces by repulsive image forces. We employ the WKB (Wentzel–Kramers–Brillouin) quantum mechanical method for the Green function of the Edwards equation to determine the adsorption equilibrium. Scaling relations are determined for the critical adsorption strength required to initiate polymer adsorption onto these low-dielectric supports. Image-force repulsion shifts the equilibrium toward the desorbed state, demanding larger surface charge densities and polyelectrolyte linear charge densities for the adsorption to take place. The effect is particularly pronounced for a planar interface in a low-salt regime, where a dramatic change in the scaling behavior for the adsorption–desorption transition is predicted. For the adsorbed state, polymers with higher charge densities are displaced further from the interface by image-charge repulsions. We discuss relevant experimental evidence and argue about possible biological applications of the results.



## I. INTRODUCTION

The adsorption of polyelectrolyte (PE) chains onto oppositely charged surfaces<sup>1–3</sup> is typically governed by electrostatic (ES) interactions between the surface and the PE. PE adsorption plays a fundamental role in biological systems and technological applications. Particular examples are DNA wrapping in nucleosome core particles,<sup>4,5</sup> RNA adsorption on the interior of viral capsids,<sup>6–8</sup> PE multilayered vesicles,<sup>9</sup> coating of colloidal particles, and papermaking. Correspondingly, it received considerable attention. *Weak* ES-driven adsorption of flexible PE chains onto planar and curved interfaces, for example, has been the subject of various theoretical<sup>10–20</sup> and computer simulation studies,<sup>21–30</sup> to mention recent ones only.

Experimentally, particularly in the group of P. Dubin, the conditions for adsorption and complex formation have been studied of both flexible and semiflexible PEs onto spherical and cylindrical micelles,<sup>31,32</sup> dendrimers,<sup>33</sup> and some oppositely charged proteins.<sup>34,35</sup> As an important result, these experiments yield the critical adsorption threshold as a function of the surface charge density, PE linear charge density, salt concentration, and temperature. The adsorption transition separates entropy-dominated free states of a polymer chain in solution from bound states in the vicinity of an adsorbing surface, which are favored by ES attraction.

The salinity of solution is a sensitive parameter to control the onset of PE adsorption. In low-salt solutions (long Debye screening lengths), the PE layers are typically more compact than in highly concentrated electrolytes. As the surface charges are shielded with increasing salt concentration, larger surface

charge densities  $\sigma$  are required to trigger adsorption. Thereby the functional relation between the critical surface-charge density and salt concentration depends on the considered geometry. For a planar surface, the critical  $\sigma$  scales with the cube of the reciprocal Debye screening length,  $\sigma \propto \kappa^3$ . For cylindrical and spherical interfaces, on the other hand, a more intricate behavior has been predicted by us recently,<sup>36</sup> with the general trends being in agreement<sup>37</sup> with a large set of data of the Dubin group.

Certain substrates for PE adsorption possess a low-dielectric constant (mica, silica particles, clay, latex particles, biological membranes, globular proteins, etc.). In this case, in addition to the direct PE-surface ES attraction, an ES repulsion of PE charges from image charges of the same sign created beneath the interface has to be taken into account. For planar and spherical surfaces, the implications of this repulsion for various PE depositional properties have been examined theoretically<sup>38,39</sup> and by computer simulations.<sup>40,41</sup> For planar surfaces, it has been shown that the image forces *inhibit* ES-driven PE adsorption, deplete the PE layers near the adsorbing interface, and can prevent surface overcharging by the adsorbed PE chains.<sup>42</sup> For a sphere, an image-force-mediated dewrapping transition of *highly charged* PEs from a spherical colloid has also been predicted.<sup>43</sup> For *weak* PE-surface adsorption, however, no consistent scheme has been proposed in the literature, to the

**Received:** May 22, 2012

**Revised:** July 7, 2012

**Published:** July 15, 2012



best of our knowledge, to describe the image charge effects for planar<sup>44,45</sup> and spherical<sup>46,47</sup> geometries at finite salt concentration.

In this article, we provide a theoretical description of the adsorption of PEs onto planar and spherical surfaces in the presence of image charges. We adopt the Edwards equation to describe the PE conformational properties and apply the ground-state dominance approximation. The resulting equation is solved by the WKB approach developed in ref 36. For both geometries, we determine the adsorption threshold as a function of image charge repulsion. Above the adsorption transition, we find a progressive *depletion* of adsorbed PE with increasing image charge interactions. Our calculations yield scaling relations for the critical adsorption strength as a function of the Debye screening length, which are rather different from the high dielectric surface case. Therefore, our calculations provide deeper insight into the adsorption process and offer qualitative explanations for the experimentally observed behavior of PE adsorption at low-dielectric surfaces.

The paper is organized as follows. In the next section, we present the general concept of the WKB method for the Edwards equation for the polymer conformational properties in the attractive field of the surface. The results for PE adsorption onto low-dielectric substrates of planar and spherical geometries are discussed in section III. In section IV, we present various relevant experimental data and argue about implications of the model assumptions applied.

## II. MODELING WEAK PE ADSORPTION

We consider weak PE-surface adsorption for PE-counterion interactions below the Manning counterion condensation threshold.<sup>48,49</sup> The PE linear charge density is denoted as  $\rho = e_0/b_0$ , where  $e_0$  is the elementary charge and  $b_0$  is the PE intercharge separation. The latter is larger than the Bjerrum length  $l_B = e_0^2/(ek_B T)$ , which is about 7 Å in water at room temperature. Here,  $\epsilon$  denotes the dielectric constant,  $T$  the temperature, and  $k_B$  is Boltzmann's constant. Both  $\sigma$  and  $\rho$  are assumed to remain constant during the adsorption process, and dilute PE solutions are considered. Similarly, the ES potential of a charged surface is calculated within the linear Poisson–Boltzmann model, which implies that the approach is only applicable up to a maximal surface charge density and above a minimal salt concentration, respectively.

The conformational properties of a flexible PE chain of length  $L$  in the mean-field potential  $V_{DH} + V_{im}$  are described by the Edwards equation

$$\left( \frac{\partial}{\partial L} - \frac{b}{6} \nabla_r^2 + \frac{V_{DH}(\mathbf{r}) + V_{im}(\mathbf{r})}{k_B T} \right) G(\mathbf{r}, \mathbf{r}'; L) = \delta(\mathbf{r} - \mathbf{r}') \delta(L) \quad (1)$$

where  $G(\mathbf{r}, \mathbf{r}'; L)$  is the probability density to find a polymer end at  $\mathbf{r}(0) = \mathbf{r}'$  and the other at  $\mathbf{r}(L) = \mathbf{r}$  and  $b$  is the polymer Kuhn length.  $V_{DH}$  is the Debye–Hückel potential of the surface, i.e., the screened PE-surface ES attraction, and  $V_{im}$  is the short-range repulsive potential of image charges. The Debye–Hückel attraction scales with the surface charge density  $\sigma$  and the PE linear charge density  $\rho$  as  $V_{DH}(x) \propto |\sigma\rho|$ ; see ref 36. The image-charge repulsion scales quadratically with the PE charge density,  $V_{im} \propto \rho^2$ , as described below. The Edwards equation can be solved by an eigenfunction expansion

$$G(\mathbf{r}, \mathbf{r}'; L) = \sum_n \Psi_n^*(\mathbf{r}') \Psi_n(\mathbf{r}) e^{-\mu_n L} \quad (2)$$

For long enough polymers (dozens of Kuhn segments), the lowest energy state  $n = 0$  gives the dominant contribution to the Green function within this expansion, where the ground-state eigenfunction  $\Psi_0(\mathbf{r})$  follows from the eigenvalue equation

$$\left( -\frac{b}{6} \nabla_r^2 + \frac{V_{DH}(\mathbf{r}) + V_{im}(\mathbf{r})}{k_B T} \right) \Psi_0(\mathbf{r}) = -\mu \Psi_0(\mathbf{r}) \quad (3)$$

Here,  $\mu$  is the eigenvalue ( $\mu > 0$  for the bound states). The first term in this equation describes the polymer conformational entropy, whereas the second term dictates to what extent the PE-surface potential confines the polymer near the interface. The monomer density distribution in the vicinity of the surface is then given by

$$n^2(\mathbf{r}) = |\Psi_0(\mathbf{r})|^2 / \int |\Psi_0(\mathbf{r})|^2 d\mathbf{r} \quad (4)$$

## III. BASIC EQUATIONS AND RESULTS

The quantum mechanical WKB approach<sup>50</sup> provides a convenient and suitable way to solve eq 3 analytically. We recently applied the WKB approach to the critical adsorption of PEs for various geometries.<sup>36,51</sup> Using the same approach, we will present the solution of the Edwards equation including the image repulsion. The reader is referred to ref 36 for details of the method. The main advantage of the WKB method is that it yields an approximate uniformly valid solution for the PE density and critical adsorption conditions for virtually *arbitrarily shaped* PE-surface interaction potentials.

**a. Low-Dielectric Half-Space.** For a unit point-like charge immersed in electrolyte solution with the dielectric constant  $\epsilon$  in front of a planar interface with a low dielectric permittivity  $\epsilon_c$

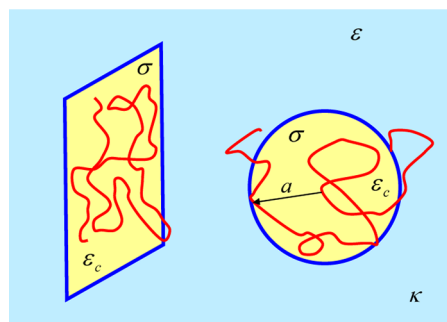


**Figure 1.** Pictorial representation of the considered adsorption geometries.

Figure 1, the screened image-charge repulsion energy<sup>52–55</sup> is given by the Onsager–Samaras result

$$E_{im}(x) = k_B T \frac{l_B \Delta e^{-2\kappa x}}{4x} \quad (5)$$

Here,  $\Delta = (\epsilon - \epsilon_c)/(\epsilon + \epsilon_c)$  is the dielectric contrast parameter ( $\Delta \approx 1$  for many realistic situations when  $\epsilon_c \ll \epsilon$ ),  $x$  is the charge-surface distance, and  $2x$  is the separation of the charge from its image of the same sign. The image repulsion thus decays twice as fast as the direct Debye–Hückel PE-surface attraction.

For a PE chain in front of such an interface, we employ a “local image charge” approximation assuming that every PE charge interacts *only* with its own image across the boundary, irrespective of the conformation adapted by the rest of the chain. As an effective PE charge interacting, we take the PE charge within *one Debye length* along the contour,  $\rho/\kappa$ . As the image repulsion decays fast with charge–charge separation, this local assumption is expected to be valid. It is particularly true for a PE chain positioned close to the adsorbing surface, so that the surface-charge separation  $x$  is smaller than the Debye screening length of the electrolyte,  $\lambda_D$ . This ensures that for a straight PE in front of a dielectric interface the contribution from the own image charge dominates over the repulsion from the next neighboring images, i.e., the relation  $e^{-2\kappa x} \gg e^{-\kappa((2x)^2 + \lambda_D^2)^{1/2}}$  applies. This is the basic motivation for cumulating all the PE charges within one Debye length along the chain contour into a single “effective” charge of magnitude  $\rho\lambda_D$  which is then responsible for image-charge repulsion. This coarse-graining of PE charges is necessary to employ the “local image charge” approximation.

Of course, one can encounter situations when the PE chain bends locally *toward* the interface and then the next neighboring image might be closer to this particular PE charge. One can avoid such cases assuming that the polymer persistence length is rather large compared to  $\lambda_D$ . Then, the chain curvature on the length scale of the separation between the local electric charges  $\lambda_D$  is rather small, diminishing the repulsion from the next-neighboring image charge below the surface. The above-mentioned locality assumption allows us to implement the WKB approach straightforwardly.

Hence, per unit PE length, the interaction potential of a chain segment at a distance  $x$  from the low-dielectric attractive surface can be written as<sup>2</sup>

$$V_{\text{DH}}(x) + V_{\text{im}}(x) = -\theta e^{-\kappa x} + \theta_{\text{im}} \frac{e^{-2\kappa x}}{\kappa x} \quad (6)$$

where

$$\theta = \frac{4\pi|\rho\sigma|}{\epsilon k_B T \kappa} \equiv \frac{\delta b}{6\kappa a^3} \quad \text{and} \quad \theta_{\text{im}} = \frac{\rho^2 \Delta}{4\epsilon k_B T}$$

with the definition

$$\delta = \frac{24\pi a^3 |\rho\sigma|}{\epsilon b k_B T} \quad (7)$$

The parameters  $\theta$  and  $\theta_{\text{im}}$  control the strength of the PE-surface attraction and the PE-(image PE) repulsion, respectively. The parameter  $\delta$  is the most important parameter of the model that characterizes the adsorption–desorption behavior of PE chains. The parameter

$$\kappa \equiv 1/\lambda_D = \sqrt{8\pi l_B n_0} \quad (8)$$

is the inverse Debye screening length in a solution of 1:1 salt with ionic concentration  $n_0$ .

In the ground state, within the WKB approach we get

$$\Psi_0''(x) - R(x)\Psi_0(x) = 0 \quad (9)$$

with the “potential” function

$$R(x) = \frac{6}{b} \left( \mu - \theta e^{-\kappa x} + \theta_{\text{im}} \frac{e^{-2\kappa x}}{\kappa x} \right) \quad (10)$$

The solution of eq 9 can be expressed in terms of Airy functions

$$\Psi_0(x) \sim \text{Ai}(\pm[3\xi/2]^{2/3})$$

where the variable  $\xi$  depends on the potential 10; see below. The plus sign corresponds to negative  $R(x)$  values and the minus sign to positive  $R$ , respectively.<sup>36</sup>

The presence of image charges gives rise to an overall PE-surface ES repulsion at small distances  $x$ . The total potential approaches the Debye–Hückel attraction far from the surface; see Figure 2. The separations at which the eigenvalue  $\mu$  is equal

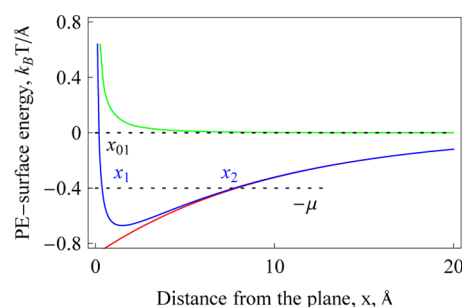


**Figure 2.** Typical shapes of the Debye–Hückel PE-surface attraction (red) and the screened PE-(image PE) repulsion energies (green), as well as their sum (blue curve). The intercepts with the eigenvalue  $\mu$  are indicated as  $x_{1,2}$ . Parameters:  $\sigma = e_0/100 \text{ Å}^2$ ,  $\rho = e_0/10 \text{ Å}$ ,  $1/\kappa = 10 \text{ Å}$ , and  $\Delta = 1$ .

to the normalized PE-surface potential are denoted as  $x_{1,2}$ . The “oscillating part” of the solution for  $\Psi_0(x)$  appears in the region between these two points of the potential; i.e., for the region where  $R(x_1 < x < x_2) < 0$ , see ref 36. The first zero at the distance  $x_1$  from the interface turns into  $x_{01}$  at the critical adsorption condition of  $\mu = 0$ , and the second crossing point is  $x_2 \rightarrow \infty$ .

This transition determines the critical parameters, where a localized polymer-density profile emerges near the interface. Physically, this threshold defines the minimal surface charge density, minimal PE linear charge density, and maximal temperature  $T$  at which the PE-surface attraction energy exceeds the entropic free energy for a free polymer far from the interface. This can be expressed in mathematical terms as a condition for the argument  $\xi$  of the Airy function that is the eigenfunction of the Edwards equation as shown in ref 36. Explicitly, the argument  $\xi(x) = \int_x^{x_2} (-R(x'))^{1/2} dx'$  for  $x > x_1$  at the adsorption transition turns into

$$\frac{\xi_c}{\sqrt{6}} = C = \int_{x_{01}}^{\infty} \sqrt{\frac{\theta}{b} e^{-\kappa x} - \frac{\theta_{\text{im}}}{b} \frac{e^{-2\kappa x}}{\kappa x}} dx \quad (11)$$

where the constant  $C$  is specified via the first zero  $ai$  of the Airy function as  $C \equiv 2|ai_1|^{3/2}/(3\sqrt{6}) \approx 0.973$ ; see ref 56. The zero  $x_{01}(\delta_c)$  follows from

$$\frac{e^{-\kappa x_{01}}}{\kappa x_{01}} = \frac{\theta}{\theta_{\text{im}}} = \frac{\delta_c b}{6a^3 \kappa \theta_{\text{im}}} \quad (12)$$

Here,  $a$  is a length scale for the planar surface and the sphere radius. The critical adsorption strength  $\delta_c$  is defined by eq 11 as the solution of the transcendental equation ( $u = \kappa x$ )

$$\delta_c = \frac{6C^2(\kappa a)^3}{\left( \int_{\kappa x_{01}}^{\infty} du e^{-u/2} \sqrt{1 - \frac{\theta_{im} 6a^3 \kappa e^{-u}}{\delta_c b}} \right)^2} \quad (13)$$

Hence, with the image forces present, the equations for  $\delta_c(x_{01})$  and  $x_{01}$  are nontrivially coupled and they can only be solved numerically.

The results show that a PE depletion near the interface caused by the image charge repulsion demands somewhat *higher* values for the critical adsorption strength  $\delta_c$ , particularly at small  $\kappa a$  values; see Figure 3. Image repulsions effectively

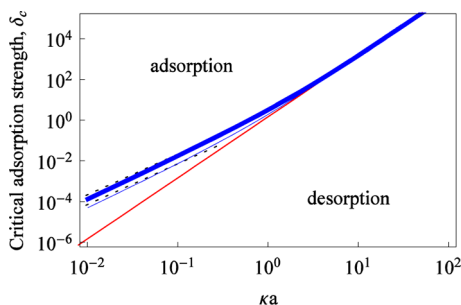


**Figure 3.** Dependence of the critical adsorption parameter  $\delta_c = 24\pi a^3 |\sigma_p| / (\epsilon \kappa_B T b)$  on solution salinity for various PE linear charge densities. Parameters:  $a = 30$  Å,  $b = 30$  Å, and  $b_0 = 10$  and  $30$  Å for thick and thin curves, respectively. Scaling asymptotes of eq 15 are shown as dotted black lines, while the adsorption–desorption transition for a plane is the red curve, eq 14.

shift PE chains into a region with a *weaker* attractive potential. In this limit, we find that  $\delta_c$  closely follows the scaling relation  $\delta_c \propto \kappa^2$ . It differs from the cubical dependence<sup>36</sup>

$$\delta_c^{\text{plane}} = 6C^2(\kappa a)^3/4 \approx 1.42(\kappa a)^3 \quad (14)$$

obtained for purely attractive PE planes (at  $\theta_{im} = 0$  or  $\epsilon_c = \epsilon$ ); see the red line in Figure 3. The crossover region between the two scaling regimes depends on the PE charge density: for highly charged PEs (smaller  $b_0$  values), the transition takes place at larger  $\kappa a$  values. Physically, eq 14 expresses the following relation. As more salt is dissolved in the buffer, the ES PE-surface attraction diminishes. To compensate for this enhanced screening and still ensure PE adsorption, the surface charge density has to grow as  $\sigma \propto \kappa^3$ . This is a well-known exact result for the planar interface,  $\delta_c^{\text{plane}} \approx 1.446(\kappa a)^3$ .<sup>10</sup>

In the presence of image repulsion, the situation is more complicated. For instance, the critical adsorption strength  $\delta_c$  at  $\kappa a \ll 1$  grows with the PE linear charge density above this planar result; see Figure 3. This somewhat paradoxical conclusion (stronger charged PEs require larger surface charge densities to get adsorbed) follows from the fact that image-charge repulsion scales as  $\propto \rho^2$ , while PE-surface attraction energy is only linear in  $\rho$ . As displayed in Figure 3, at low salt, the influence of image charge repulsion on  $\delta_c$  is quite dramatic. In the limit of  $\kappa a \ll 1$ , one can estimate the dominant scaling dependence on the amount of added salt as

$$\delta_c \propto \frac{6Ca^3}{4b_0} \sqrt{\frac{l_B \Delta}{b}} \kappa^2 \quad (15)$$

while at high salinities  $\delta_c \rightarrow \delta_c^{\text{plane}}$ .

Also, the distance  $x_{01}$ , at which the direct ES PE-surface attraction and PE–PE image-force repulsion are equal, exhibits

a peculiar dependence on  $\kappa a$ ; see Figure 4. This distance quantifies the extent by which the density profiles of the

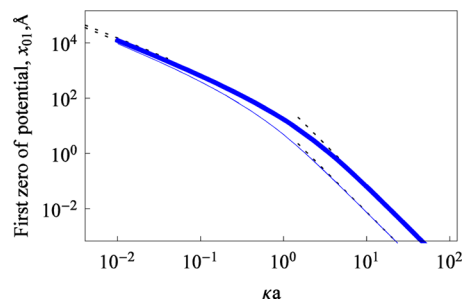


**Figure 4.** Scaling regimes for the first zero of the PE-surface interaction potential. The scaling relations eq 16 (at high salt) and eq 17 (at low salt) are shown as black dotted lines. Parameters and notations are the same as in Figure 3.

adsorbed PEs are displaced from the interface by the image-force repulsion. We find that  $x_{01}$  decreases with increasing  $\kappa$ , because at high salt concentrations the influence of the image-charge potential is screened already in close vicinity to the interface. Naturally, PE chains with *higher* charge densities yield larger  $x_{01}$  and *stronger* PE depletion from the surface, see Figure 4, again due to the quadratic dependence of image repulsion on PE charge density.

We can rationalize these two scaling regimes for  $x_{01}$  as follows. At large  $\kappa$  values, when the influence of image forces is strongly screened, we get  $\delta_c \rightarrow \delta_c^{\text{plane}}$  and

$$x_{01} \propto \frac{l_B \Delta}{C^2 b b_0^2} \kappa^{-3} \quad (16)$$

In the opposite limit of low salinity, we obtain

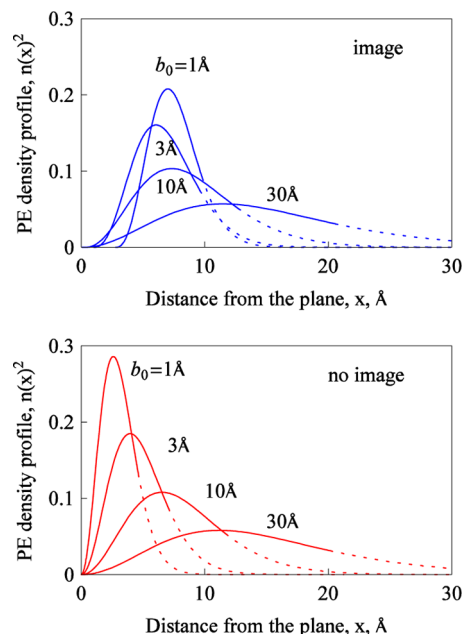


**Figure 5.** Polymer density profiles near an adsorbing plane with (blue curves) and without (red curves) the image-force repulsion, plotted for different PE linear charge densities  $e_0/b_0$ . Other parameters are the same as in Figure 2.



$$x_{01} \propto -\ln \left[ C b_0 \sqrt{\frac{b}{l_B \Delta}} \kappa \right] / \kappa \quad (17)$$

Both scaling asymptotes are shown as dotted lines in Figure 4. The PE linear charge densities used in Figures 3 and 4 are below the Manning counterion condensation threshold,  $b_0 > l_B$ .

Typical normalized density profiles  $n(x)^2$  for PE chains in the adsorbed state, for the parameters well above the adsorption transition, are shown in Figure 5, for comparison with and without the image charge repulsion. The general trend for the image-free case is that the profiles are somewhat narrower. The PE chains are getting more localized near the surface as the PE-surface attraction  $\propto |\sigma| \rho l$  grows (as  $b_0$  decreases). For  $\epsilon_c \ll \epsilon$ , on the contrary, a stronger PE-(image PE) repulsion shifts the PE adsorbed layer progressively away from the surface, favoring a desorbed state of the polymer chain and a more swollen adsorbed PE layer.

**b. Low-Dielectric Spherical Colloid.** The calculation of screened image-charge effects for a PE near an adsorbing spherical surface is more involved, as compared to the planar geometry. In the absence of an electrolyte, the induced self-image charges inside a low-dielectric sphere of radius  $a$  have been computed in refs 57 and 58. This exact solution encompasses an infinite number of images generated by a dielectric discontinuity at  $r = a$ . Due to a fast decay of this ES repulsion, often the *first image* of the same sign and a “cumulative” effective image of the opposite charge are enough to grasp the important physics. This is particularly valid for a charge *far* from the sphere. One more new feature compared to the plane is that the positions of the appearing image charges depend on the charge separation from the boundary.

The presence of an electrolyte further complicates the situation. Here, however, we want to keep the consideration on a qualitative level, avoiding solving the full and complicated image charge ES boundary problem. We rather suppose that, similarly to the planar surface, in a salt solution, the Coulomb image-charge potential<sup>59</sup> is screened with a decay length half as short as  $\lambda_D$ . With such an exponential shielding, the model with only two “effective” image charges becomes even more applicable. Note also that the procedure of discretizing PE charges every Debye length is likely less accurate than this two-image-charges ansatz.

For an elementary charge  $e_0$  located at a distance  $r$  from the center of a low-dielectric sphere, the screened ES interaction from the two image charges inside the sphere can be approximated as

$$E_{\text{im}}^{\text{sph}}(r) = k_B T l_B \Delta \frac{a}{r} \left( \frac{e^{-2\kappa r(1-a^2/r^2)}}{2r(1-a^2/r^2)} - \frac{e^{-2\kappa r}}{2r} \right) > 0 \quad (18)$$

Here, the first term is the *repulsion* from the image charge of the same sign  $e_0 \Delta a/r$  at separation  $a^2/r$  from the sphere center. The second term is the *attraction* by the image charge of the same magnitude but opposite sign located at  $r = 0$ . Physically, we can expect that, as the solid angle at which a low-dielectric object is “seen” by the real charge  $e_0$  is reduced when we go from a plane to a sphere, the corresponding image-charge repulsion will be progressively reduced. As a consequence, the image-charge effect on the PE critical adsorption characteristics will diminish too. Also, this solid angle decreases as the separation  $d$  from a charge to the interface increases; see Figure 6. For large spheres and small  $d$ , the energy  $E_{\text{im}}^{\text{sph}}(a + d)$

approaches the Onsager–Samaras result<sup>53</sup> for the planar surface  $E_{\text{im}}(d)$ ; see eq 5.

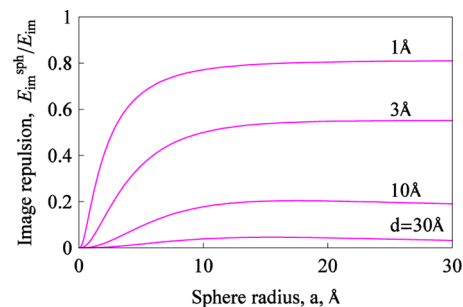


**Figure 6.** Image-charge repulsion for various separations  $d$  of a PE from a low-dielectric sphere, relative to the image repulsion from a planar interface. Parameters:  $1/\kappa = 10$  Å and  $\Delta = 1$ .

Per unit polymer length, the interaction potential of a PE chain in front of a low-dielectric oppositely charged surface can then be written as

$$V_{\text{DH}}^{\text{sph}}(r) + V_{\text{im}}^{\text{sph}}(r) = -\frac{\delta b}{6a(1+\kappa a)r} + \frac{2\theta_{\text{im}}a/r}{\kappa r} \left( \frac{e^{-2\kappa r(1-a^2/r^2)}}{1-a^2/r^2} - e^{-2\kappa r} \right) \quad (19)$$

Analogously to the planar case, the eigenfunction  $\varphi(r) = r\Psi_0(r)$  for the ground state obeys the equation<sup>36</sup>

$$\varphi''(r) - R(r)\varphi(r) = 0 \quad (20)$$

where now

$$R(r) = \frac{6}{b} \left( \mu - \frac{\delta b}{6a(1+\kappa a)r} + \frac{2\theta_{\text{im}}a/r}{\kappa r} \left( \frac{e^{-2\kappa r(1-a^2/r^2)}}{1-a^2/r^2} - e^{-2\kappa r} \right) \right) \quad (21)$$

The critical adsorption condition is defined through the oscillatory part of the eigenfunction that can mathematically be described by  $\xi_c/\sqrt{6} = \int_{\kappa r_{01}}^{\infty} (-R(u)/6)^{1/2} du/\kappa$  or

$$C = \int_{\kappa r_{01}}^{\infty} du \sqrt{\frac{\delta}{6a\kappa(1+\kappa a)u} - \frac{2\theta_{\text{im}}\kappa a/u}{b\kappa^2} \left( \frac{e^{-2u}e^{2(\kappa a)^2/u}}{u(1-(\kappa a/u)^2)} - \frac{e^{-2u}}{u} \right)} \quad (22)$$

with  $u = \kappa r$ . The critical adsorption strength is then

$$\delta_c = \frac{6\kappa a(1+\kappa a)C^2}{e^{\kappa a}F(a, \delta_c)^2} \quad (23)$$

where

$$F(a, \delta_c) = \int_{\kappa r_{01}}^{\infty} du \sqrt{\frac{e^{-u}}{u} \sqrt{1 - \frac{6a(1+\kappa a)}{\delta_c \kappa e^{\kappa a}} \frac{2\theta_{\text{im}}\kappa a/u}{b} \left( \frac{e^{-u}e^{2(\kappa a)^2/u}}{1-(\kappa a/u)^2} - e^{-u} \right)}}} \quad (24)$$

Similarly to the adsorbing plane, the distance  $r_{01}(\delta_c)$ , defined as the first zero of the integrand of the function  $F$ , and the critical

adsorption strength  $\delta_c$  are found via a numerical solution of the two coupled equations. The solution procedure often requires some tuning, depending on the model parameters. Note also that, in the absence of a dielectric discontinuity,  $\kappa a$  is a universal parameter<sup>36</sup> that couples the surface curvature and solution salinity. This is no longer the case in the presence of image forces.

In the absence of image charges  $\theta_{\text{im}} = 0$ , we get  $r_{01} = a$ ,  $F = \int_{\kappa a}^{\infty} du (e^{-u}/u)^{1/2} = 2\pi \operatorname{erfc}[(\kappa a/2)^{1/2}]$  that yields the previous result<sup>36</sup>

$$\delta_c = \frac{6\kappa a(1 + \kappa a)C^2}{2\pi e^{\kappa a} \operatorname{erfc}^2(\sqrt{\kappa a/2})} \quad (25)$$

where  $\operatorname{erfc}(y) = 1 - \operatorname{erf}(y)$  is the complementary error function. Using its expansions for  $\kappa a \ll 1$ , we recover the linear scaling for the adsorption strength at low salt

$$\delta_c \approx 6C^2\kappa a/(2\pi) \approx 0.904(\kappa a)^1 \quad (26)$$

while, for  $\kappa a \gg 1$ , the planar limit is attained, with a stronger dependence  $\delta_c \propto (\kappa a)^3$ .

The results for  $\delta_c$  are shown in Figure 7. Analogously to a planar surface, as the PE charge density increases, the adsorbing

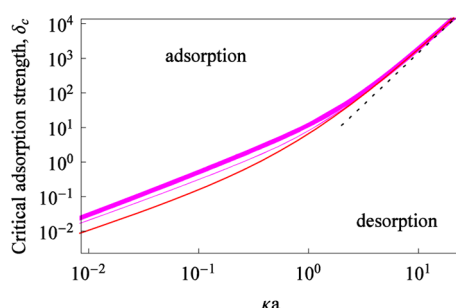


**Figure 7.** Critical parameter  $\delta_c$  for PE adsorption onto a low-dielectric sphere. The red curve corresponds to a water-filled sphere, eq 25, and the dotted line indicates the scaling relation  $\delta_c^{\text{plane}} \propto (\kappa a)^3$  for a planar surface, eq 14. Parameters:  $a = 30 \text{ \AA}$ ,  $b = 30 \text{ \AA}$ , and  $b_0 = 10$  and  $30 \text{ \AA}$  (for thick and thin curves, respectively). More highly charged PEs require larger  $\delta$  and  $\sigma$  values to get adsorbed.

polymer experiences stronger image repulsion and therefore  $\delta_c$  increases. The effect is, however, much weaker and does not affect the scaling behavior in the limit  $\kappa a \ll 1$ . This is an important difference from the planar situation.

The dependence of the zero-potential point on  $\kappa a$  is shown in Figure 8 for various values of the PE charge density. At low

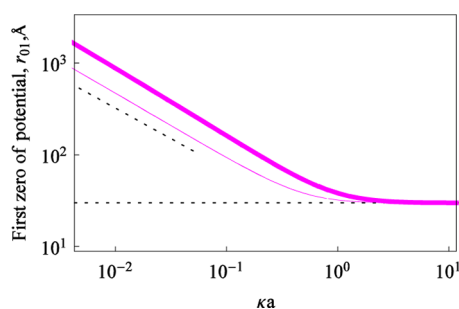


**Figure 8.** The first zero of the interaction potential between a PE and a low-dielectric sphere. The dotted line is  $r_{01} \propto (\kappa a)^{-2/3}$ . Parameters and notations for the curves are the same as in Figure 7.

salt concentrations, the first zero of the PE-surface potential exhibits a

$$r_{01} \propto (\kappa a)^{-2/3} \quad (27)$$

scaling, while at high salt it approaches the sphere radius, i.e.,  $r_{01} \rightarrow a$ . Overall, the extent of image-force induced PE displacements from the adsorbing sphere is much weaker than for a planar boundary; compare Figures 4 and 8. For increasing sphere radii (at a constant PE charge density), we observe the expected enhancement of image repulsion, which gives rise to larger  $\delta_c$  values (not shown).

#### IV. DISCUSSION AND OUTLOOK

In this study, we have examined the effects of a dielectric discontinuity on electrostatically driven PE adsorption onto planar and spherical surfaces. We have demonstrated that image charge repulsion causes a stronger “exclusion” of PE chains from a planar surface as compared to a spherical interface. PE chains with higher charge densities  $\rho$  are displaced further from the surface, because of  $\rho^2$  dependence of the image repulsion. Physically, this implies that larger surface charge densities and/or lower temperatures are necessary to induce PE adsorption onto a low-dielectric surface, as compared to a case without a dielectric contrast. In addition, in the low-salt limit, the scaling behavior of  $\delta_c(\kappa)$  is altered for the planar interface, while only the magnitude of  $\delta_c$  grows for the spherical boundary. This is the key result of the paper.

In the simplistic adsorption model implemented above, we neglected a number of features of real systems that can modify our conclusions. Many of these aspects, however, complicate the problem heavily, so that it becomes only amenable to a numerical solution.

- We consider PE adsorption in the “static” field of the dielectric surface, without any influence of the adsorbed chains on the potential profile of the surface. Several self-consistent models with a coupling of PE and ion distributions next to the interface have been developed.<sup>60–63</sup>
- We employ the Debye–Hückel theory to calculate the potential of a charged surface in an electrolyte interacting with dissolved PE chains. This model is known to have a number of inherent limitations, particularly at high surface charges and low-salt concentrations. Under such conditions, the ES potentials might well exceed the 25 mV margin allowed for this linear Poisson–Boltzmann model. This follows from the expressions for the linearized ES surface potential for planar ( $4\pi\sigma/\epsilon\kappa$ ) and spherical ( $4\pi\sigma/\epsilon\kappa)(\kappa a/(1 + \kappa a))$  geometries. When comparing our predictions for the critical adsorption parameter  $\delta_c$  with the experimental data,<sup>31–35,64</sup> this point is to be remembered. At large surface charge densities or low salt concentrations, the full nonlinear Poisson–Boltzmann theory has to be employed, both for the ES potential of the interface<sup>65</sup> and for the PE chains.<sup>66</sup>
- This potential is set to be the *only* source of PE attraction to the surface, with no short-range non-ES contracts, etc. Moreover, no close-packing and specific effects of electrolyte ions near the charged surface<sup>67,68</sup> have been taken into account.
- We assume that the weakly charged PE chains remain *nearly Gaussian* polymers in the course of adsorption,

with their conformational properties being only weakly perturbed. This severe assumption will definitely turn invalid at large  $\sigma$  values and at low salinities (at the conditions of stronger adsorption). Under these conditions, the excluded-volume effects and PE–PE charge repulsion become important.

- The PE-surface adsorption is assumed to be “weak” in the entire range of parameters. The model predictions, e.g., for the width  $w$  of the adsorbed PE layer,  $w \propto \delta^{-1/3}$ ,<sup>36</sup> are thus only valid for quite extended PE layers, for the parameters not too far from the adsorption–desorption transition.
- The persistence length  $b/2$  of the considered PE chains describes the mechanical properties of the polymer. The ES component to the bending persistence of flexible PEs,  $l_p^{\text{el}}$ , is known to be salt-dependent, i.e.,  $l_p^{\text{el}} \propto \kappa^{-\gamma}$ , with the exponent  $\gamma \approx 1$ . This fact can be incorporated in the final results for the critical adsorption strength in order to obtain a more realistic  $\delta_c(\kappa)$  dependence.<sup>11,15</sup>
- The layers formed by adsorbed PEs lack any internal structure in the model. We neglect both the intrachain ES repulsion and possible interchain repulsions in the adsorbed layer. These can affect PE adsorption as a function of added salt, particularly for dense PE layers; see, e.g., the treatment in ref 2 and the discussion below.
- The polymer chains in the ground-state dominance limit are effectively *infinitely long*, so no PE length effects can be envisaged from this approach. The treatment of shorter PE chains requires also accounting for contributions from the excited energy states in the Green function expansion.
- A “local image charge” approximation is used. A more accurate approach should involve a summation over all the images created beneath the surface by adsorbing PE chains. This implies integration over the PE profiles giving rise to integro-differential equations for determining a self-consistent solution for the polymer profile.

Our theoretical predictions for PE exclusion from the low-dielectric adsorbing boundaries are in line with some computer simulations in the salt-free limit. They reveal a depletion of adsorbed PE chains in front of a low-dielectric planar surface, see Figures 1 and 2 in ref 42, as well as a reduction in the surface coverage by adsorbed polymers. Since the polymers are effectively very long in our model, we *cannot reproduce* the effect of an enhanced depletion of longer chains as revealed from simulations. The physics behind this enhancement is a roughly quadratic length dependence of the image repulsion energy. Such “dielectric exclusion” of adsorbing PEs is also reminiscent of a displacement of the atmosphere of mobile electrolyte ions in the diffuse layer being formed near a charged low-dielectric surface; see Figure 4 in ref 69 and Figures 8 and 9 in ref 58.

We could not find data of systematic measurements of the effect of surface curvature on PE adsorption and the critical adsorption conditions for low-dielectric interfaces. One insightful experimental study of adsorption of flexible PEs onto functionalized oppositely charged polystyrene latex particles is, however, presented in ref 70. It underlines the importance of a number of effects that cannot be captured in the current model (see the list above).

The study of ref 70 reveals, e.g., that the amount of adsorbed PEs exhibits a *nonmonotonic* dependence on the amount of

added salt. Upon increase of salinity in the range 0.01–0.1 M, more PE chains were adsorbed on the interface, while further increase of KCl up to 0.3 M triggered some PE desorption. This initial counterintuitive increase of PE surface coverage has been attributed to a progressive *screening* of PE–PE repulsions in the adsorbed layer. Upon further increase of salt, the ES PE-surface attraction is progressively diminished too, which diminishes adsorption. Simultaneously, a competitive adsorption of small mobile ions to the interface might take place and the PE ES persistence length could be reduced at elevated salt concentrations. Thus, at moderate-to-high salt concentrations, the confinement of a charged polymer near the interface becomes entropically costly, because of a larger chain conformational freedom. At the same time, the ES PE-surface attraction is diminished, the probability of forming weakly bound polymer loops or tails is enhanced, and thus the equilibrium is rather shifted toward desorbed polymer configurations. All these effects require more involved models of PE adsorption, beyond the scope of the current study.

Finally, the theoretical trends predicted above might be applicable to the adsorption of single-stranded RNA molecules inside many spherical and some filamentous viral capsids. The inner surfaces of spherical RNA viruses for a number of families are rich in strongly positively charged flexible polypeptides; see, e.g., refs 6 and 71. They guide the adsorption of negatively charged flexible single-stranded RNA genomes in close vicinity of the capsid surface, ensuring a proper assembly kinetics and robustness of final viral particles. The viral shells themselves are composed of capsomer proteins, which self-assemble largely via hydrophobic interactions. This indicates a low value of dielectric permittivity in the shell layer of these one-protein-thick nanocontainers. Recent theoretical models proposed for this electrostatically driven polymer encapsulation process<sup>72,73</sup> might thus require a treatment of image charges, as proposed in the present paper.

## AUTHOR INFORMATION

### Corresponding Author

\*E-mail: a.cherstvy@gmail.com.

### Notes

The authors declare no competing financial interest.

## ACKNOWLEDGMENTS

The work was supported by the German Research Foundation, DFG grant CH 707/5-1 to A.G.C. Enlightening discussions with P. Dubin are acknowledged.

## REFERENCES

- (1) Netz, R. R.; Andelman, D. *Phys. Rep.* **2003**, *380*, 1.
- (2) Dobrynin, A. V.; Rubinstein, M. *Prog. Polym. Sci.* **2005**, *30*, 1049.
- (3) Dobrynin, A. V. *Curr. Opin. Colloid Interface Sci.* **2008**, *13*, 376.
- (4) Luger, K.; et al. *Nature* **1997**, *389*, 251.
- (5) Cherstvy, A. G. *J. Phys. Chem. B* **2009**, *113*, 4242.
- (6) Belyi, V. A.; Muthukumar, M. *Proc. Natl. Acad. Sci. U.S.A.* **2006**, *103*, 17174.
- (7) Forrey, C.; Muthukumar, M. *J. Chem. Phys.* **2009**, *131*, 105101.
- (8) Cherstvy, A. G. *Phys. Chem. Chem. Phys.* **2011**, *13*, 9942.
- (9) Caruso, F.; et al. *Macromolecules* **1999**, *32*, 2317.
- (10) Wiegand, F. W. *J. Phys. A: Math. Gen.* **1977**, *10*, 299.
- (11) Muthukumar, M. *J. Chem. Phys.* **1987**, *86*, 7230.
- (12) Baumgartner, A.; Muthukumar, M. *J. Chem. Phys.* **1991**, *94*, 4062.
- (13) van Goeler, F.; Muthukumar, M. *J. Chem. Phys.* **1994**, *100*, 7796.
- (14) Linse, P. *Macromolecules* **1996**, *29*, 326.

- (15) Shafir, A.; Andelman, D.; Netz, R. R. *J. Chem. Phys.* **2003**, *119*, 2355.
- (16) Winkler, R. G.; Cherstvy, A. G. *Phys. Rev. Lett.* **2006**, *96*, 066103.
- (17) Winkler, R. G.; Cherstvy, A. G. *J. Phys. Chem. B* **2007**, *111*, 8486.
- (18) Man, X.; et al. *Macromolecules* **2008**, *41*, 5451.
- (19) Licer, M.; Podgornik, R. *J. Phys.: Condens. Matter* **2010**, *22*, 414102.
- (20) Wang, Z.; et al. *Macromolecules* **2011**, *44*, 8607.
- (21) Chodanowski, P.; Stoll, S. *J. Chem. Phys.* **2001**, *115*, 4951.
- (22) Kong, C. Y.; Muthukumar, M. *J. Chem. Phys.* **1998**, *109*, 1522.
- (23) Welch, P.; Muthukumar, M. *Macromolecules* **2000**, *33*, 6159.
- (24) Messina, R.; Holm, C.; Kremer, K. *J. Polym. Sci., Part B* **2004**, *42*, 3557.
- (25) Ulrich, S.; et al. *Macromolecules* **2005**, *38*, 8939.
- (26) Stoll, S.; Chodanowski, P. *Macromolecules* **2002**, *35*, 9556.
- (27) Kaellrot, N.; Linse, P. *J. Phys. Chem. B* **2010**, *114*, 3741.
- (28) Ulrich, S.; et al. *Curr. Opin. Colloid Interface Sci.* **2006**, *11*, 268.
- (29) Cao, Q.; et al. *Soft Matter* **2011**, *7*, 506.
- (30) Carnal, F.; Stoll, S. *J. Phys. Chem. B* **2011**, *115*, 12007.
- (31) McQuigg, D. W.; et al. *J. Phys. Chem.* **1992**, *96*, 1973.
- (32) Feng, X. H.; et al. *Macromolecules* **2001**, *34*, 6373.
- (33) Kayitmazer, A. B.; Shaw, D.; Dubin, P. L. *Macromolecules* **2005**, *38*, 5198.
- (34) Cooper, C. L.; et al. *Biomacromolecules* **2006**, *7*, 1025.
- (35) Kayitmazer, A. B.; et al. *Biomacromolecules* **2010**, *11*, 3325.
- (36) Cherstvy, A. G.; Winkler, R. G. *J. Phys. Chem. Chem. Phys.* **2011**, *13*, 11686.
- (37) Cherstvy, A. G.; Winkler, R. G. *J. Chem. Phys.* **2006**, *125*, 064904.
- (38) Netz, R. R.; Joanny, J.-F. *Macromolecules* **1999**, *32*, 9013.
- (39) Netz, R. R. *Eur. Phys. J. E* **2001**, *5*, 189.
- (40) Dobrynin, A. V.; Rubinstein, M. *J. Phys. Chem. B* **2003**, *107*, 8260.
- (41) Messina, R. *J. Phys.: Condens. Matter* **2009**, *21*, 113102.
- (42) Messina, R. *Phys. Rev. E* **2004**, *70*, 051802.
- (43) Netz, R. R.; Joanny, J.-F. *Macromolecules* **1999**, *32*, 9026.
- (44) Buyukdagli, S.; Manghi, M.; Palmeri, J. *Phys. Rev. E* **2010**, *81*, 041601.
- (45) Hatlo, M. M.; Curtis, R. A.; Lue, L. *J. Chem. Phys.* **2008**, *128*, 164717.
- (46) Curtis, R. A.; Lue, L. *J. Chem. Phys.* **2005**, *123*, 174702.
- (47) Hatlo, M. M.; Lue, L. *Soft Matter* **2008**, *4*, 1582.
- (48) Manning, G. S. *Macromolecules* **2001**, *34*, 4650.
- (49) Manning, G. S. *J. Phys. Chem. B* **2007**, *111*, 8554.
- (50) Langer, R. E. *Phys. Rev.* **1937**, *51*, 669.
- (51) Cherstvy, A. G. *Biopolymers* **2012**, *97*, 311.
- (52) Wagner, C. Z. *Phys.* **1924**, XXV, 474.
- (53) Onsager, L.; Samaras, N. N. T. *J. Chem. Phys.* **1934**, *2*, 528.
- (54) Croxton, T.; et al. *Can. J. Chem.* **1981**, *9*, 1998.
- (55) Manciu, M.; Ruckenstein, E. *Adv. Colloid Interface Sci.* **2003**, *105*, 63.
- (56) Odijk, T. *Macromolecules* **1980**, *13*, 1542.
- (57) Linse, P. *J. Phys. Chem.* **1986**, *90*, 6821.
- (58) Messina, R. *J. Chem. Phys.* **2002**, *117*, 11062.
- (59) Cherstvy, A. G. *J. Phys. Chem. B* **2007**, *111*, 7914.
- (60) Podgornik, R. *J. Phys. Chem.* **1992**, *96*, 884.
- (61) Borukhov, I.; Andelman, D.; Orland, H. *J. Phys. Chem. B* **1999**, *103*, 5042.
- (62) Podgornik, R. *J. Chem. Phys.* **2003**, *118*, 11286.
- (63) Podgornik, R. *J. Polym. Sci., Part B* **2004**, *42*, 3539.
- (64) Sennato, S.; Truzzolillo, D.; Bordi, F. *Soft Matter* **2012**, DOI: 10.1039/c2sm25576f.
- (65) Verwey, E. J. W.; Overbeek, J. Th. G. *Theory of the Stability of Lyophobic Colloids*; Elsevier: New York, 1948.
- (66) Fuoss, R. M.; Katchalsky, A.; Lifson, S. *Proc. Natl. Acad. Sci. U.S.A.* **1951**, *37*, 579.
- (67) Ben-Yaakov, D.; et al. *J. Phys.: Condens. Matter* **2009**, *21*, 424106.
- (68) Ben-Yaakov, D.; et al. *Curr. Opin. Colloid Interface Sci.* **2011**, *16*, 542.
- (69) Lue, L.; Linse, P. *J. Chem. Phys.* **2011**, *135*, 224508.
- (70) Shubin, V.; et al. *Colloid Polym. Sci.* **1997**, *275*, 655.
- (71) Siber, A.; et al. *Phys. Chem. Chem. Phys.* **2012**, *14*, 3746.
- (72) Wang, J.; Muthukumar, M. *J. Chem. Phys.* **2011**, *135*, 194901.
- (73) Ting, C. L.; et al. *Proc. Natl. Acad. Sci. U.S.A.* **2011**, *108*, 16986.